Electronic Supplementary Material (ESI) for New Journal of Chemistry.

Supporting Information

Self-assembled $Mg(OH)_2$ gels driving to MgO nanoribbons

Thiago Galeote Tabuti[b], Lorena Portela Brazuna[b], Rafael Gagliardi Antoneli[a], Eduardo do Valle Ricardo[b], Rebeca Bacani[a], Dayane Batista Tada[b] and Eduardo Rezende Triboni*[a]

[a] Laboratory of Nanotechnology and Process Engineering, Chemistry Department, Universidade de São Paulo, Lorena, SP-Brasil.

[b]Laboratory of Nanomaterials and Nanotoxicology, Instituto de Ciência e Tecnologia, Universidade Federal de São Paulo, SJC, SP-Brasil.

SI.1 – Materials, gel preparation and further analysis

Materials

Magnesium nitrate hexahydrate ($Mg(NO_3)_2.6H_2O$, 96 %), magnesium sulphate ($MgSO_4.7H_2O$), isopropanol (99 %), sodium hydroxide (NaOH, 98 %), and glycerol (99.5 %) were purchased from Synth (Brazilian company) and used without further purification. Water was doubly distilled and deionized through a Milli-Q system.

Preparation of Mg hydroxide/oxide nanoparticles in Glycerol Isopropanol solvent – a Survey

Standard gel preparation: firstly, glycerol:isopropanol 3:1 mole ratio solvent (GI) was mixed before salt dissolution. After that 0.1 mol of $Mg(NO_3)_2.6H_2O$ was dissolved into GI (30 mL) at room temperature, and then 0.2mol of NaOH aqueous solution (5mL) was added at once under stirring at 600 rpm. Mixing these reagents a whitish $Mg(OH)_2$ gel was formed almost immediately, Fig. 1a. In order to remove glycerol, isopropanol and residual salts, $Mg(OH)_2$ gel was washed with large amount of deionized water four times under stirring (200 ml in each time), Fig.S1 b- c.

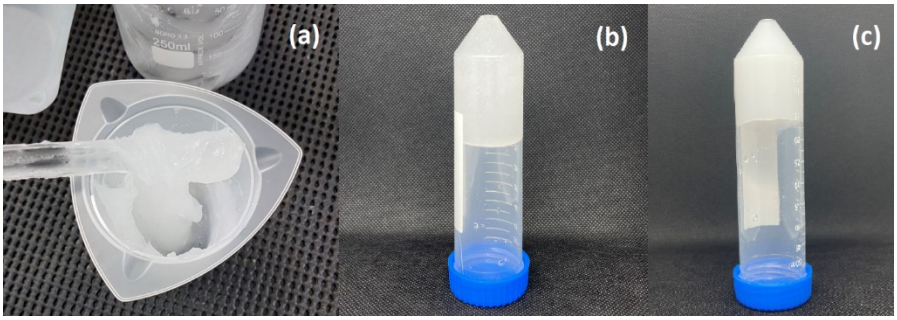

Figure S1. $Mg(OH)_2$ gel: (a) as-prepared and (b) centrifuged, and (c) washed and centrifuged.

In addition, at varying concentration of the magnesium salt, while keeping 1:2 salt:base ratio, $Mg(OH)_2$ gels having different apparent viscosities from stiff to viscous solutions were obtained as amount of reagent decreased as well as distinct translucency, Fig.2 a-c. Notice, $MgSO_4.7H_2O$ also provides a good gel being an alternative salt. However, a better investigation must be made regarding rheological properties and salt interference on gel features and on the MgO nanoparticles characteristics as well.

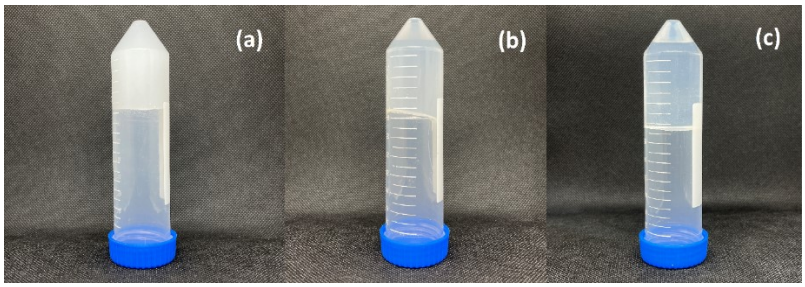

Figure S2. $Mg(OH)_2$ gel (Mg^{2+} salt mole amount in 30 mL glycerol/isopropanol): (a) sulfate precursor, (b) 2/5 Mg^{2+} nitrate, and (c) 1/5 Mg^{2+}nitrate.

Xerogel preparation

Washed $Mg(OH)_2$ hydrogel was dried in an oven at 70°C for 4 h. A white powder was formed, and PXRD analysis indicates Brucite $Mg(OH)_2$ structure (space group P-3m1, number 164), see SI-2, Fig.S3.

Lyophilization (freeze-dried)

$Mg(OH)_2$ hydrogel was frozen for 3 h at -60 °C to then promoting the lyophilization for 15 h at 40 below zero under pressure of 0.09 mbar. A white powder was formed, and PXRD analysis indicates Brucite $Mg(OH)_2$ structure (space group P-3m1, number 164), see SI-2, Fig.S3.

Thermal treatment and infrared

$Mg(OH)_2$ xerogel and hydrogel were calcinated in an oven at 400°C for 3h under atmospheric pressure in order to obtain MgO nanoparticles (Space group Fm-3m, number 225), see SI-2, Fig.S4.

SI.2 - PXRD analysis

Structural characterization for $Mg(OH)_2$ and MgO are presented on the Table S1 and S2. X'Pert Highscore from PANalytical/Malvern was utilized for the whole profile fitting of the XRD profiles. ICSD database was used for the structural model, the profiles' intensities were simulated with a pseudo-Voigt function without asymmetry and the background was fitted with a 10^{th}

polynomial function. Isotropic temperature factors were considered, and the samples' displacement and absorption were also corrected. Average crystallite size was calculated from Scherrer formula and the lattice microstrain was determined by Stokes-Wilson equation [1-7]. $Mg(OH)_2$ and MgO diffractograms are presented Fig.S3 and S4.

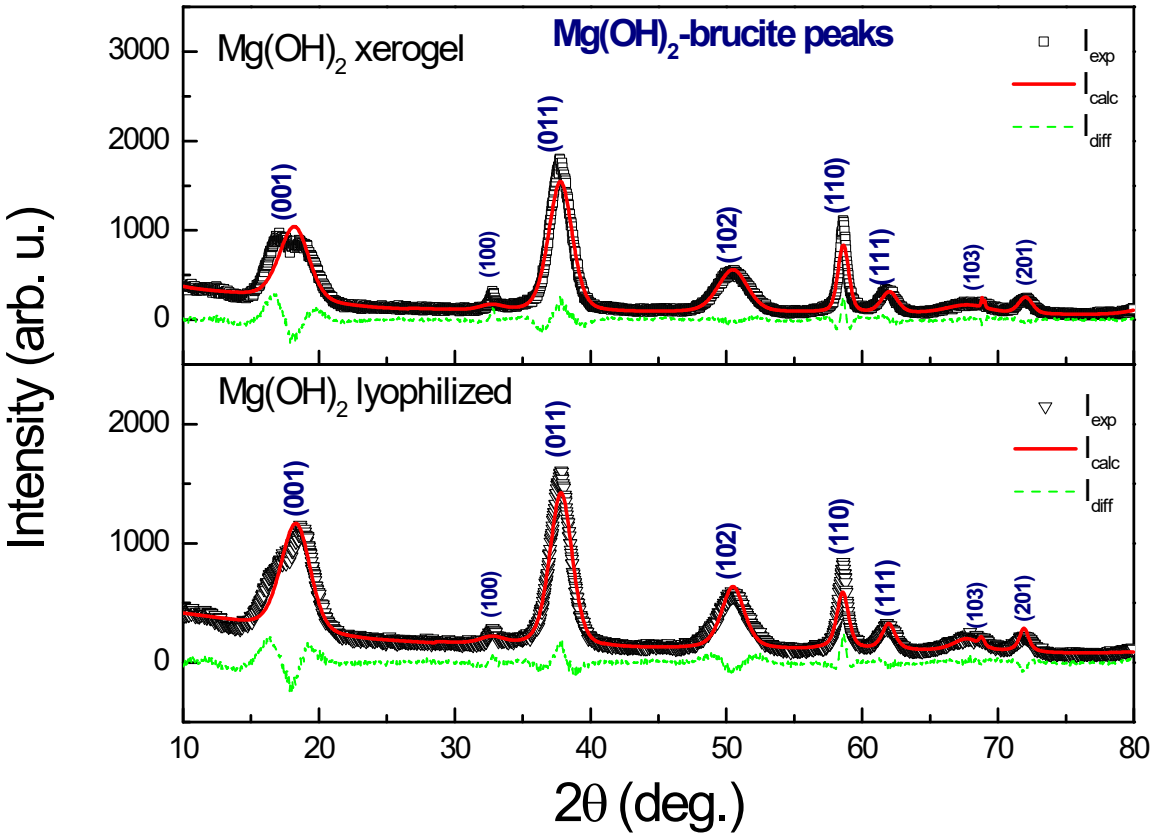

Figure S3. $Mg(OH)_2$ structures. Symbols I_{exp} experimental data; I_{calc} calculated profile from Rietveld analysis, I_{diff} difference between calculated and experimental profiles.

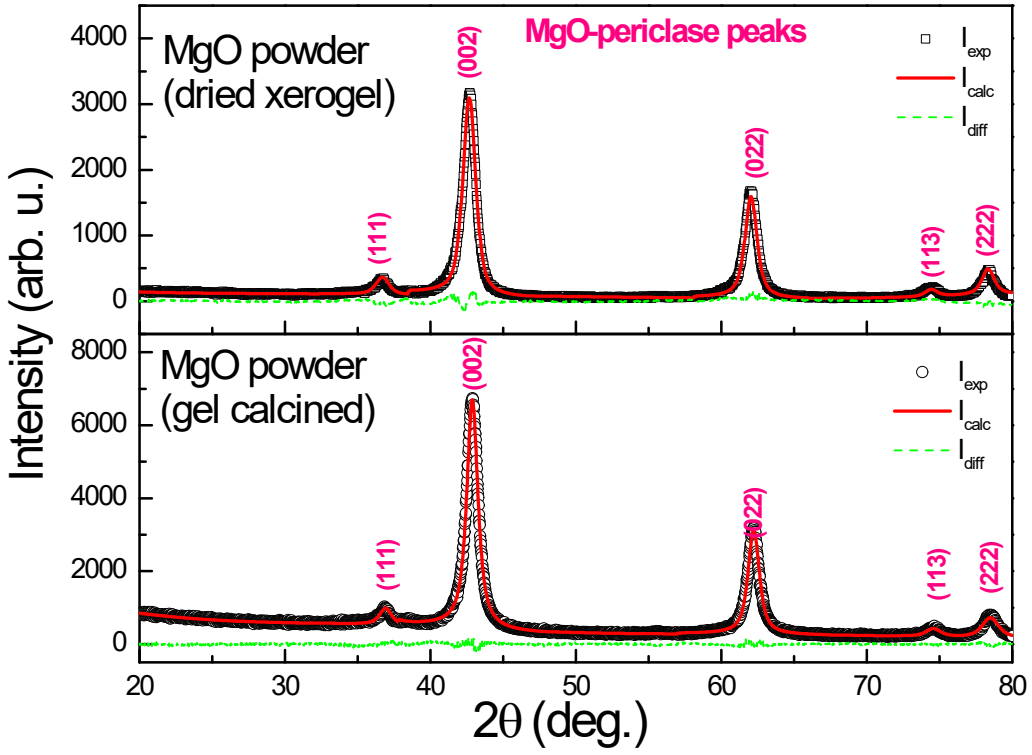

Figure S4. MgO structures. Symbols I_{exp} experimental data; I_{calc} calculated profile from Rietveld analysis, I_{diff} difference between calculated and experimental profiles.

Brucite $Mg(OH)_2$ (space group P-3m1, number 164) is a layered material made of a lattice with a central plane of Mg atoms surrounded by planes of OH groups in the (00l) direction [9], Fig. S5. For $Mg(OH)_2$ some different strategies were employed in order to fit the whole pattern due to anisotropic broadening of the (00l) peaks. Lyophilized and xerogel $Mg(OH)_2$ structures stretch the (hk0) planes and give rise to anisotropic crystallites with an similar preferred orientation, though some structural differences may be noted. Different thermal treatments, drying and lyophilization, led to few differences in the lattices: lyophilized $Mg(OH)_2$ particles have higher lattice volume while those from xerogel have smaller crystallite sizes owing to larger lattice parameters and micro-strains (Table S1).

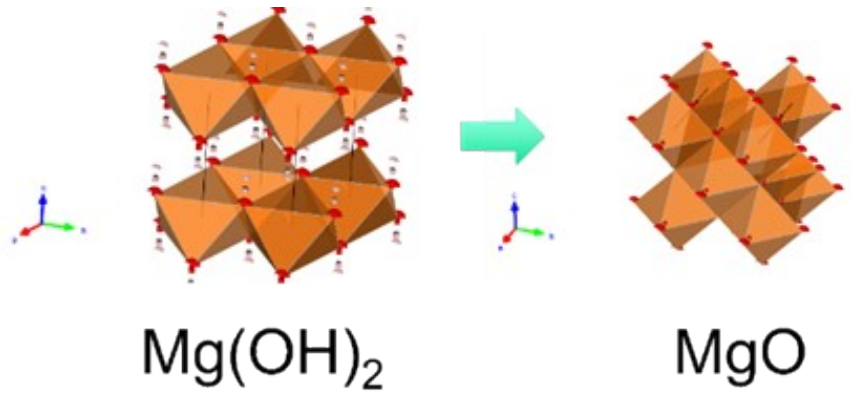

Figure S5. $Mg(OH)_2$ and MgO crystal structures (VESTA software) [8].

MgO periclase cubic structure (Space group Fm-3m, number 225) is usually formed by the $Mg(OH)_2$ decomposition around 300 ºC [10-13]. Although MgO particles showed different morphologies their XRD profiles did not show issues regarding anisotropic broadening, but still retaining a small preferred orientation of (hk0) peaks for both of leave- or ribbon-shaped morphologies [9,10]. Lattice strain and volume had very small differences, indicating a robust MgO formation after calcination of the xerogel or hydrogel.

Table S1. *X-Ray Diffraction complete results:* samples' crystallographic phases, phase fraction, phases' lattices parameters (a,b, c) and cell volume (V). Scherrer average crystallite size ($D_{(hkl)}$) and, lattice microstrain (ε).

Sample	***Phase weight (%)***	***Lattice parameters***		***V_{cell} (Å³)***	***$D_{(hkl)}$ (nm)***	***ε (%)***
		a=b (Å)	**c (Å)**			
xerogel	100% brucite	3.144(9)	4.672(8)	40.00(4)	8(3)	2.0(7)
hydrogel lyophilized	100% brucite	3.150(11)	4.811(4)	41.33(5)	7.0(3)	1.6(9)
Dried xerogel	100% periclase	a=b=c= 4.2194(6)		75.12(9)	11.0(4)	0.45(4)
Hydrogel calcined	100% periclase	a=b=c= 4.2229(5)		75.30(8)	8.5(7)	0.39(7)

Table S2. Rietveld convergence indices for each sample.

Sample	*Rexp*	*Rp*	*Rwp*	*GOF*	*X²*
xerogel	6.2	12.16	15.16	5.98	2.45
hydrogel lyophilized	5.96	10.05	13.02	4.77	2.18
Dried xerogel	6.96	8.58	11.71	2.83	1.68
Hydrogel calcined	6.98	5.75	7.93	1.29	1.14

SI-3 – SEM

$Mg(OH)_2$ particles obtained after lyophilization of the hydrogel prepared directly in water. Individual particles are seen with a very trapezoidal shapes, Fig.S6.

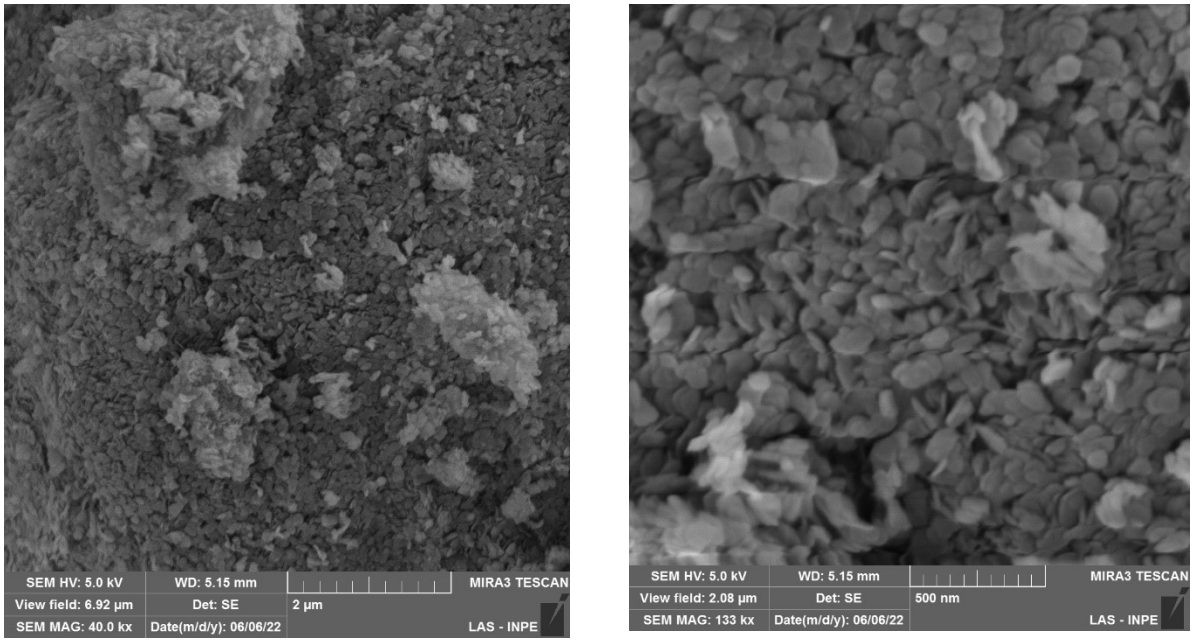

Figure S6. SEM images of the lyophilized $Mg(OH)_2$ gel.

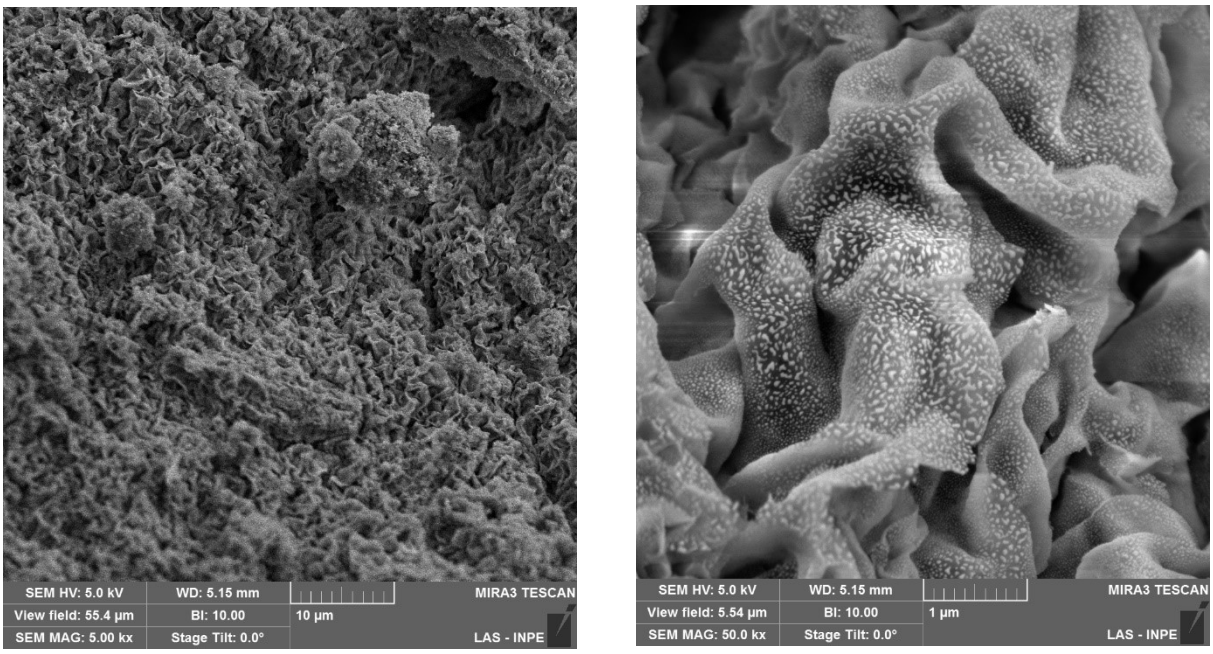

Figure S7. SEM images of MgO ribbons from calcined hydrogel that was prepared with Mg_2SO_4.

SI-4 - EDS/TEM images

In order to characterize the formation of MgO spheres EDS spectra was collected, Fig. S8.

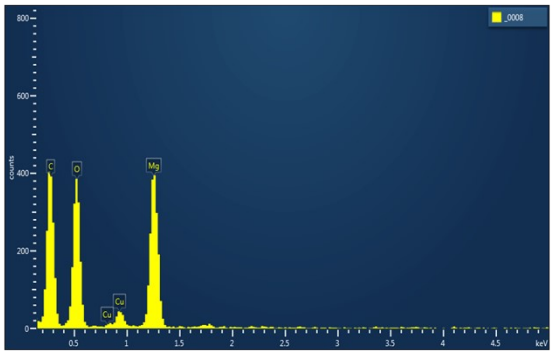

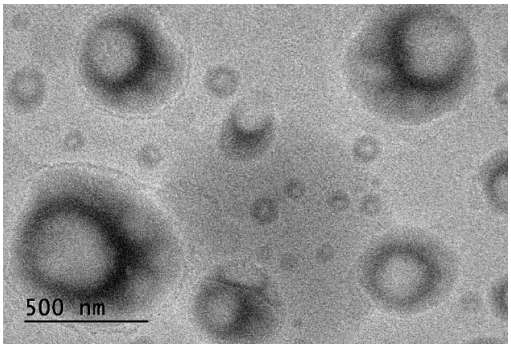

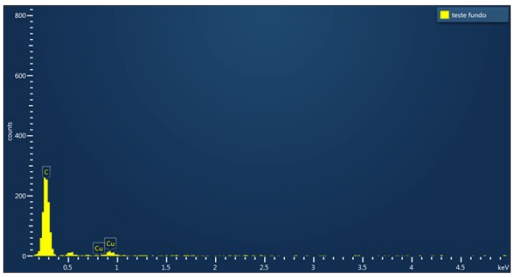

Figure S8. Top: EDS/TEM measurements: confirmation of MgO spherical particles after sonication. Bottom: grid background EDS image.

SI-5 – Dynamic Light Scattering (DLS) measurements

Table S3. DLS results for the MgO nanoribbons after sonication.

Sample	sonication time (min)	Average particle size (nm)
The same sample described in fig.5 (main article)	0	not measured
	20	185 ± 58
	60 (run 1)	110 ± 30
	60 (run 2)	185 ± 36

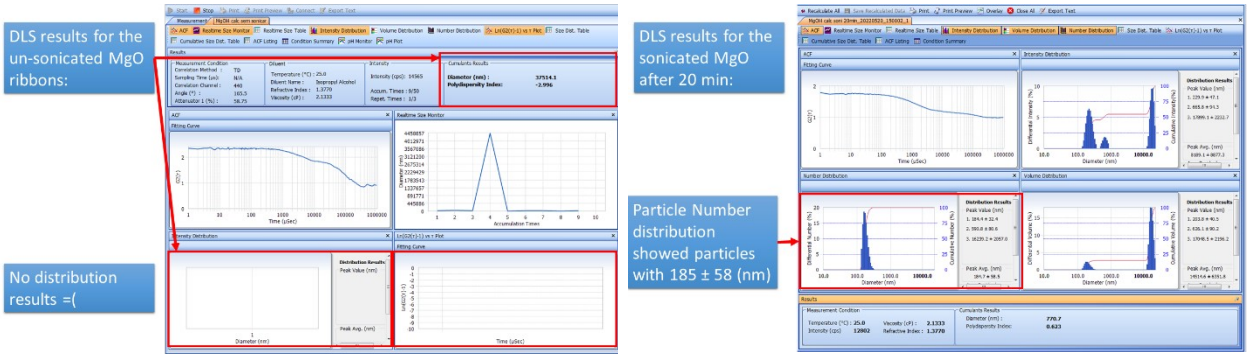

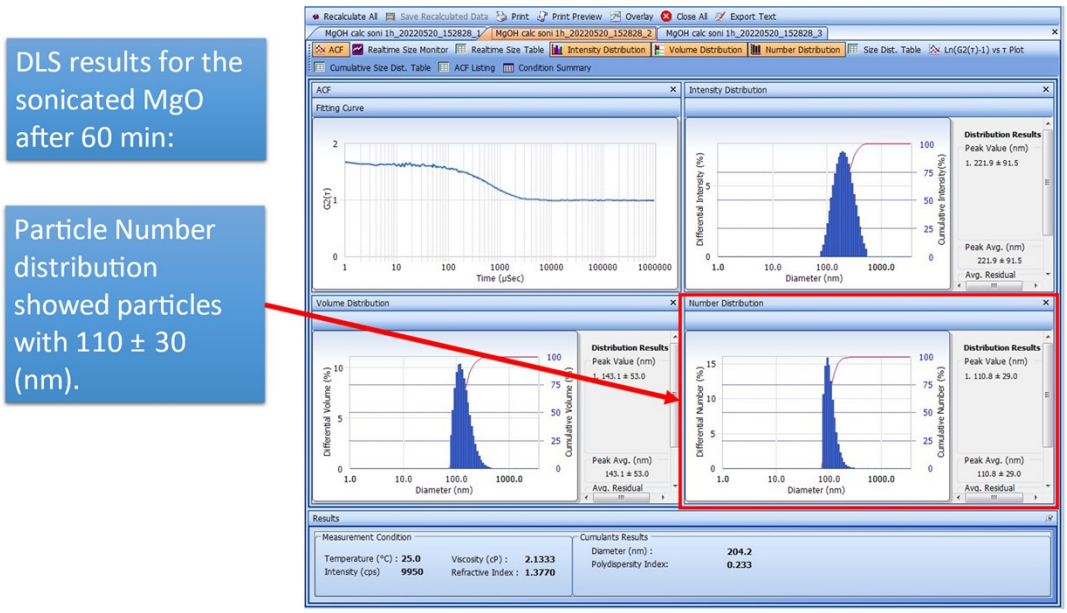

Figure S9. Above: MgO before sonication, after 20 min of sonication. Below: DLS after 60 min of sonication, showing the average particle size.

SI-6 – Nitrogen Adsorption Analysis (NAI) measurements

The NAI (Fig. S10) showed an open hysteresis with small pores format [13,14]. The specific surface area after 60 min of sonication was 45 m²/g with adsorbed volume at P/P_0 = 0,95 of 0,085 cm³/g. The pore size distribution showed an average pore size of ~20 nm.

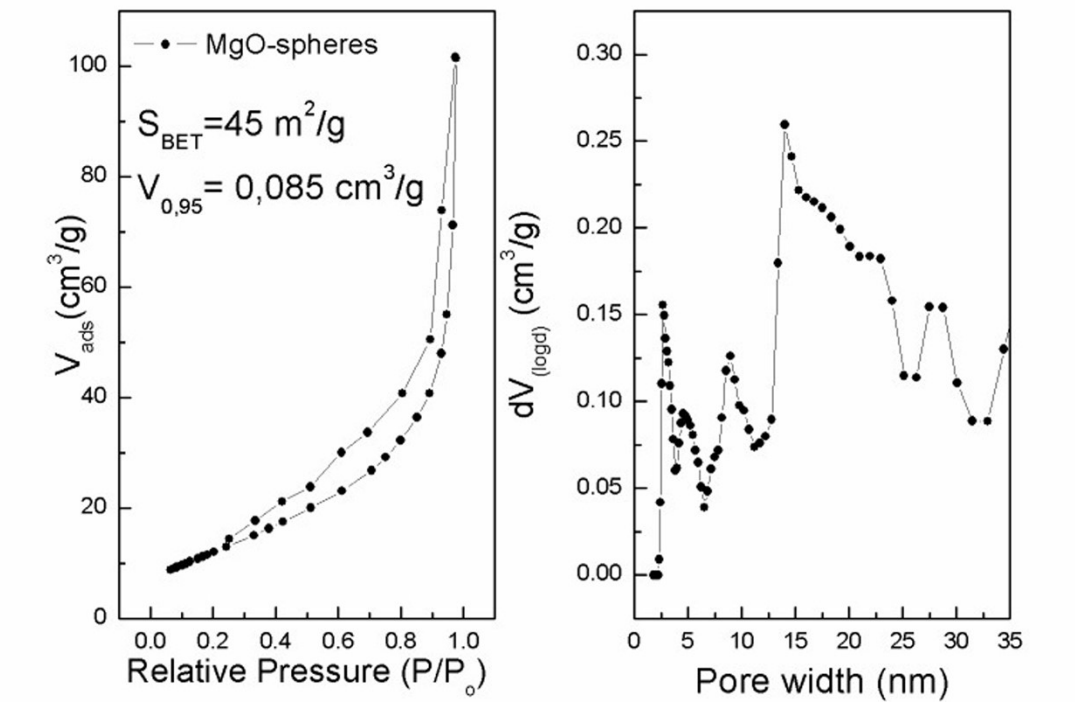

Figure S10: Left: Nitrogen adsorption isotherm. Right: Pore size distribution.

Instruments and Methods

The X-ray diffraction (XRD) experiments were carried out with the dried nanoparticles in powder form with a PANalytical Empyrean diffractometer with a PIXEL3D detector, copper tube (λ=1.5418 Å) and a Ni filter. The equipment operated at 40 kV and 30 mA, with 2θ from 20° to 70° with a 0.02° step, counting time of 5 s/step. ize the difference between the observed and simulated powder diffraction patterns. The Rietveld R values are used as indicators of the model convergence.

Electron microscopy images were obtained to evaluate nanoparticles size and morphology. Scanning electron microscopy (SEM) images were obtained with a field emission electron microscopy JEOL JSM-7401F with an acceleration tension of 5.0 kV, SEI secondary electron detector, working distance ranging from 3.0 mm and resolution of 1.5 nm and High-resolution transmission electronic microscopy (HRTEM) images were obtained with a JEM-2100-JEOL microscope with 0.23 nm of resolution point with 80 to 200 kV accelerating voltage. For the experiments, 1 mg of hydroxide/oxide magnesium nanoparticles were dispersed in 10 mL of isopropanol by sonication in an ultrasonic bath for 1 h.

Freeze drying Edwards Super Modulyo Edwards super modulyo freeze dryer. DLS experiments were DLS Delsa Nano C Particle Analyzer da Beckman Coulter. DLS sample preparation consisted of isopropanol suspensions.

N_2 adsorption-desorption measurements were recorded on a Quantachrome Nova Win adsorption analyzer, sample after sonication for 60 min was previously sonicated in isopropanol and dried in a petri dish on a fume hood for 2h. Sample was degassed at 200 ºC and isotherms were measured at 77 K. Specific surface area was calculated via Brunauer Emmett Teller (BET) method and the pore size distribution was determined using Density Functional Theory (DFT) method, assuming a slit-shaped pore geometry. The total pore volume ($V_{0.98}$) was determined from the aggregation of N_2 vapor adsorbed at a relative pressure of 0.99.

References

[1] R. A. Young, “The Rietveld Method” (International Union of Crystallography Monographs on Crystal), Ox- ford University Press, USA, 1995.

[2] L. B. McCusker, R. B. V. Dreele, D. E. Cox, D. Loueor, P. Scardi, “Rietveld refinement guidelines”, Journal of Applied Crystallography 32 (1999) 36–50.

[3] E. Jansen, W. Schafer, G. Will, “R values in analysis of powder diffraction data using Rietveld refinement”, Journal of Applied Crystallography 27 (1993) 492–496.

[4] R. J. Hill, R. X. Fischer, “Profile agreement indices in Rietveld and pattern-fitting analysis”, Journal of Ap- plied Crystallography 23 (1990) 462–468.

[5] J.-F. B´erar, P. Lelann, “E.S.D.’s and estimated probable error obtained in Rietveld refinements with local correlations”, Journal of Applied Crystallography 24 (1991) 1–5.

[6] B. H. Toby, “R factors in Rietveld analysis: How good is good enough?”, Powder Diffraction 21 (1), (2006) 67-70

[7] “The HighScore Suite From Phase Identification to Rietveld Analysis The HighScore Suite The Most Comprehensive Powder Diffraction Software.” n.d.

[8] Momma, Koichi, and Fujio Izumi. 2011. “VESTA 3 for Three-Dimensional Visualization of Crystal, Volumetric and Morphology Data.” *Journal of Applied Crystallography* 44 (6): 1272–76. https://doi.org/10.1107/S0021889811038970.

[9]AF. Moodie and C.E. Warble - Journal of Crystal Growth 74 (1986) 89-100

[10] Pallon et al. *J. Mater. Chem. A*, 2015,3, 7523-7534

[11] Hanlon et al. CrystEngComm, 2015, 17, 5672

[12] V. G. Tsirel'son, A. S. Avilov, Y. A. Abramov, E. L. Belokoneva, R. Kitaneh and D. Feil, Acta Crystallogr., Sect. B: Struct. Sci., 1998, 54, 8;

[13] Prieur, Damien, Walter Bonani, Karin Popa, Olaf Walter, Kyle W. Kriegsman, Mark H. Engelhard, Xiaofeng Guo, et al. 2020. “Size Dependence of Lattice Parameter and Electronic Structure in CeO2 Nanoparticles.” *Inorganic Chemistry* 59 (8): 5760–67. https://doi.org/10.1021/acs.inorgchem.0c00506.

[14] S. Brunauer, P. H. Emmet, and E. Teller, “Adsorption of gases in multimolecular layers,” Journal of the American Chemical Society 60 (1938) 309–319.

[15] E. P. Barrett, L. G. Joyner, and P. P. Halenda, “The determination of pore volume and area distributions in porous substances. I. computations from nitrogen isotherms,” Journal of the American Chemical Society 73 (1951), no. 1, 373–380.

[16] R. I. Masel, Principles of Adsorption and Reaction on Solid Surfaces. John Wiley & Sons Inc., 1996.